

# **Dark Matter in Compact Objects (TBD)**

Michael Virgato  
0000-0002-8396-0896

Submitted in total fulfilment  
of the requirements of the degree of

Doctor of Philosophy

School of Physics  
The University of Melbourne

XXX XXX

Produced on archival quality paper.

Copyright © XXX Michael Virgato

All rights reserved. No part of the publication may be reproduced in any form by print, photoprint, microfilm or any other means without written permission from the author.

# **Abstract**

DM in COs Heat up Maybe See



# Publications

Refs. [1–6] below are the journal publications, and preprints authored or co-authored during my PhD candidature. The authors are listed alphabetically in all of the titles.

## Journal papers and preprints

- [1] Papers



# **Declaration**

This is to certify that

1. the thesis comprises only my original work towards the PhD except where indicated in the preface;
2. due acknowledgement has been made in the text to all other material used;
3. the thesis is less than 100,000 words in length, exclusive of tables, maps, bibliographies and appendices.

---

Michael Virgato, XXX XXX



# Preface

We don't know what DM is. Can NSs constrain it?



# Acknowledgements

Why did I do this?



# Contents

<b>List of Figures</b>	<b>xiv</b>
<b>List of Tables</b>	<b>xvi</b>
<b>1 A Primer on Compact Objects</b>	<b>1</b>
1.1 Structure Equations from General Relativity . . . . .	2
1.2 White Dwarfs . . . . .	5
1.2.1 The FMT Equation of State . . . . .	5
1.2.2 Observational Status . . . . .	10
1.3 Neutron Stars . . . . .	12
1.3.1 Observational Status . . . . .	15
1.3.2 Choices of Neutron Star Equation of State . . . . .	16
<b>Definition of Symbols and Abbreviations</b>	<b>19</b>



# List of Figures

1.1	Electron number density (top left), chemical potential (top right), and escape velocity (bottom) radial profiles for the carbon WDs with FMT EoS in Table 1.1. The radial distance of each profile has been normalised to the radius of the star. . . . .	9
1.2	Mass-Radius relation of WDs calculated from the FMT EoS in the zero temperature approximation (dark blue), at $10^5$ K (yellow), $10^7$ K (orange), and $10^8$ K (red), together with observed WDs from Gaia EDR2 observations [15] (light blue dots). . . . .	11



# List of Tables

- 1.1 Four configurations for white dwarfs composed of carbon, with an FMT EoS. Shown are the central densities,  $\rho_c$ , stellar mass  $M_\star$  and radius  $R_\star$ , and escape velocity at the edge of the WD,  $v_{\text{esc}}$ . . . . . 8



# 1

## A Primer on Compact Objects

Within the cores of stars exists a delicate balance between the gravitational force of its mass wanting to collapse in on itself, and the outward pressure generated by thermonuclear fusion of light elements. This fusion process begins with the burning of hydrogen to form helium. Eventually, the hydrogen is depleted, allowing gravity to temporarily overcome the outward pressure leading to the core contracting. As this occurs, the gravitational potential energy is converted to thermal energy and the core eventually becomes hot enough to facilitate helium burning.

This cycle continues as heavier and heavier elements are formed within the ever-increasingly hot stellar core. If the star is heavy enough, iron will eventually be formed from the burning of silicon. As the fusion of iron nuclei is an endothermic process, it will not occur spontaneously. Whatever the mass of the star, eventually it will no longer be able to support the fusion of these heavier elements. Without a sufficient fuel source, the core will collapse under its own gravity leading to the death of the star.

What comes after this depends on the mass of the progenitor stars. Very light stars,  $\lesssim 0.5M_{\odot}$ , have lifetimes much longer than the age of the universe, and so are uninteresting to our current discussion. Moderately heavy stars,  $1M_{\odot} \lesssim M_{\star} \lesssim 8M_{\odot}$ , will continue burning fuel until the outer layers of the star are dispersed as it expands, leaving a carbon-oxygen (CO) core. The core will begin to collapse until the Fermi degeneracy of the ultrarelativistic electrons is great enough to reestablish equilibrium, resulting in a White Dwarf (WD).

Heavy stars,  $\gtrsim 8M_{\odot}$ , spectacularly end their lives in a type-II supernova event. This occurs when the core of the star exceeds the Chandrasekhar mass of  $1.4M_{\odot}$ , which cannot be supported by electron degeneracy pressure. The core itself will then collapse, leading to a shockwave that ejects the majority of the mass of the star. All that will remain is an extremely dense core supported by neutron degeneracy

pressure, a Neutron Star (NS). If the star was so massive that the gravitational forces overcome even the neutron degeneracy pressure, then the core collapses into a black hole.

These three stellar corpses (white dwarfs, neutron stars, and black holes) are collectively known as compact objects, as they have masses similar to or larger than our Sun, compressed into much smaller bodies with significantly larger surface gravities. These objects do not have a source of fuel, and spend the rest of their lives cooling down. For the remainder of this thesis, we will only be interested in white dwarfs and neutron stars and refer to these collectively as compact objects, excluding black holes from this term.

This chapter is dedicated to discussing the structure and composition of these objects<sup>1</sup>.

## 1.1 Structure Equations from General Relativity

The highly dense matter comprising neutron stars and white dwarfs leads to extremely strong gravitational fields being produced by the stars. As such, modeling the structure of these objects falls into the domain of General Relativity (GR). Here we review the structure of static, spherically symmetric stars.

The assumption that the mass distribution of the star is spherically symmetric leads to the metric taking the form

$$ds^2 = -d\tau^2 = -B(r)dt^2 + A(r)dr^2 + r^2d\Omega^2, \quad (1.1)$$

with  $d\tau$  the proper time interval, and  $A(r)$ ,  $B(r)$  are functions only of the radial coordinate and are often written as

$$A(r) = e^{2\Lambda(r)}, \quad B(r) = e^{2\Phi(r)}. \quad (1.2)$$

These functions are subject to the condition that at distances far from the star space-time becomes flat, leading to the boundary conditions

$$\lim_{r \rightarrow \infty} A(r) = \lim_{r \rightarrow \infty} B(r) = 1. \quad (1.3)$$

The matter that comprises the star is modeled as a perfect fluid, meaning we are neglecting any shear stresses and energy transport within the star. Such a fluid is described by its pressure  $P(r)$ , density  $\rho(r)$ , and number density,  $n(r)$ , as well as the 4-velocity of the fluid  $u^\mu(r)$ . Being a static fluid, the only non-zero component

---

<sup>1</sup>As this work is written by a particle physicist, I wish to apologise to my astrophysics colleagues for what is to come.

of this velocity is the time component, which is fixed through  $g_{\mu\nu}u^\mu u^\nu = -1$  to be  $u^t = 1/\sqrt{B(r)}$ . These quantities are then used to construct the stress-energy tensor for the star, which takes the form

$$T^{\mu\nu} = (\rho + P)u^\mu u^\nu + Pg^{\mu\nu}. \quad (1.4)$$

The microphysics underlying the matter interactions are encoded in an equation of state (EoS) that relates the various thermodynamic quantities. This is typically given by expressing the pressure as a function of the density,  $P(\rho)$ . It is often more convenient to parameterise the EoS by the number density of baryons,  $n_b$ , and the entropy per baryon,  $s$ , such that

$$P = P(n, s), \quad \rho = \rho(n, s). \quad (1.5)$$

The dependence on  $s$  turns out to be trivial in most scenarios involving compact objects, such as those considered here. The pressure in these stars arises from the degeneracy of the nucleons in NSs or the electrons in WDs, rather than from the thermal motion of the constituents that will be frozen out at low temperatures. This is the case for temperatures much lower than the Fermi energy of the system, with typical values of  $E_F \sim 10$  MeV in NSs or  $\sim 1$  MeV in WDs, corresponding to temperatures of  $T_* \sim 10^{11}$  K and  $\sim 10^{10}$  K respectively. As these stars are expected to cool well below these temperatures quickly after formation, the entropy can be taken to be zero throughout the star. This allows us to reduce the two-parameter EoS to a simpler one-parameter one,

$$P = P(n_b, s = 0) = P(n_b), \quad \rho = \rho(n_b, s = 0) = \rho(n_b). \quad (1.6)$$

The structure of the star is therefore determined by the quantities  $A(r)$ ,  $B(r)$ ,  $P(r)$ ,  $\rho(r)$ , and  $n_b(r)$ . This system is determined by applying the Einstein field equations,  $G^{\mu\nu} = 8\pi T^{\mu\nu}$ , together with the conservation of energy-momentum,  $T^{\mu\nu}_{;\nu} = 0$ , the EoS relations Eqs. 1.6, and the appropriate boundary conditions. The structure equations that come out of this analysis were first discovered concurrently by Tolman [7] and by Oppenheimer and Volkoff [8], and so are known as the TOV equations. They take the form

$$\frac{dP}{dr} = -\rho(r)c^2 \left[ 1 + \frac{P(r)}{\rho(r)c^2} \right] \frac{d\Phi}{dr}, \quad (1.7)$$

$$\frac{d\Phi}{dr} = \frac{GM(r)}{c^2 r^2} \left[ 1 + \frac{4\pi r^3 P(r)}{M(r)c^2} \right] \left[ 1 - \frac{2GM(r)}{c^2 r} \right]^{-1}, \quad (1.8)$$

$$\frac{dB}{dr} = 2B(r) \frac{d\Phi}{dr}, \quad (1.9)$$

where  $M(r)$  is related to the metric factor  $A(r)$  through

$$A(r) = \left[ 1 - \frac{GM(r)}{c^2 r} \right]^{-1}, \quad (1.10)$$

and is interpreted as the mass contained within a radius  $r$ . It obeys the mass equation

$$\frac{dM}{dr} = 4\pi r^2 \rho(r), \quad M(0) = 0, \quad (1.11)$$

that arises from the  $\mu = \nu = 0$  component of the Einstein field equations. These equations are the general relativistic versions of the hydrostatic equilibrium equations of regular stellar structure, with Eq. 1.7 reducing to the familiar

$$\frac{dP}{dr} = -\frac{GM(r)}{r^2} \rho(r), \quad (1.12)$$

in the Newtonian limit,  $GM(r)/c^2 r \ll 1$ .

The radius of the star,  $R_*$ , is identified as the point at which the pressure and density vanish,  $P(R_*) = \rho(R_*) = 0$ . In the region outside the star,  $r > R_*$ , the total mass remains constant at the total mass of the star,  $M(r \geq R_*) = M_*$ , and so the only non-trivial structure functions are the metric factors. Solving Eq. 1.9 with  $P(r) = 0$  and constant  $M(r)$  for  $B(r)$  becomes elementary while the result for  $A(r)$  is trivial, leaving us with

$$A(r) = \left[ 1 - \frac{GM_*}{c^2 r} \right]^{-1}, \quad B(r) = 1 - \frac{GM_*}{c^2 r}, \quad \text{for } r > R_*, \quad (1.13)$$

and the metric reduces to the familiar Schwarzschild metric outside the star. Continuity of the metric at  $r = R_*$  enforces a second boundary condition for  $B(r)$ ,

$$B(R_*) = 1 - \frac{GM_*}{c^2 R_*}. \quad (1.14)$$

The final boundary condition required is the central pressure  $P(0) = P_c$ , or equivalently the central density/baryon number density. This is the only free parameter in the system and hence, for a given EoS, uniquely determines the stellar structure. All stars generated by an EoS can therefore be represented as a one-parameter sequence, typically represented as the mass-radius relation for the model.

Given all the above, we can write a simple recipe for constructing a model of a compact object:

1. Select an EoS to describe the constituent matter.

2. Specify the central pressure of the star,  $P_c$ .
3. Integrate the coupled system of differential equations 1.7, 1.8, 1.11 from the centre of the star outward until the pressure vanishes.
4. Use the boundary condition Eq. 1.14 to normalise the metric function  $B(r)$ .

In general, additional quantities will be present in the EoS, such as chemical potentials or the speed of sound, that may be subject to additional constraints. These quantities will need to be calculated at each step of the integration alongside the other EoS quantities.

## 1.2 White Dwarfs

The fate of main sequence stars of mass below  $M_\star \lesssim 8M_\odot$  is to end their life cycles as a white dwarf. Consequently, these compact stellar remnants, which are supported against gravitational collapse by electron degeneracy pressure, are the most abundant stars in the Galaxy ( $\gtrsim 90\%$ ). They are born at very high temperatures and cool down over billions of years. Observations of the coldest WDs therefore contain information on the star formation history of the Galaxy.

The vast majority of observed WDs are composed primarily of carbon and oxygen, plus small traces of elements heavier than helium. At the extremely high densities found in WDs  $\sim 10^6 - 10^{10} \text{ g cm}^{-3}$ , electrons are strongly degenerate and determine the WD equation of state (EoS) and internal structure. The stellar core resembles a Coulomb lattice of ions surrounded by degenerate electrons, which implies that the WD core is isothermal and a very good thermal conductor. The degenerate core is enclosed by a thin envelope that accounts for  $\lesssim 1\%$  of the total mass [9].

The outer layers form an atmosphere that is rich in lighter elements such as hydrogen or helium, where the exact composition depends on the evolution of the WD progenitor and changes as the WD cools. This atmosphere is non-degenerate and extremely opaque to radiation, with an EoS that is subject to finite temperature effects.

### 1.2.1 The FMT Equation of State

In the limit of zero temperature, the simplest way to obtain the WD EoS is to assume an ideal Fermi gas of degenerate electrons, for a WD that is primarily composed of a single element. Corrections to the non-interacting electron picture were introduced early by Salpeter [10]. By introducing the Wigner-Seitz (WS) cell

approximation and assuming point-like nuclei, Salpeter obtained an analytical EoS that accounts for interactions between electrons and ions as well as other Coulomb corrections. These corrections, in general, depend on the chemical composition of the star.

More recently, it has been shown that the treatment of matter at high pressures presented by Feynman, Metropolis and Teller [11] can be extended to consistently take into account weak interactions and relativistic effects [12, 13], and incorporates Coulomb corrections in a more natural manner than the Salpeter EoS. The resulting Feynman-Metropolis-Teller (FMT) EoS is obtained by considering a relativistic Thomas-Fermi model within Wigner-Seitz cells of radius  $R_{\text{WS}}$ . For degenerate, relativistic, electrons, the equilibrium condition is that the Fermi energy,  $E_e^F$ , is constant within the cell,

$$E_e^F = \sqrt{(p_e^F)^2 + m_e^2} - m_e - eV(r) = \text{constant}, \quad (1.15)$$

where  $V(r)$  is the Coulomb potential inside the cell,  $p_e^F$  is the electron Fermi momentum,  $m_e$  is the electron mass and  $e$  is the electric charge. To obtain an integrable solution for the energy density near the origin, it is necessary to introduce a finite size for the nucleus, with radius  $R_c = \Delta\lambda_\pi Z^{1/3}$ , where  $\lambda_\pi$  is the pion Compton wavelength,  $\Delta \approx (r_0/\lambda_\pi)(A/Z)^{1/3}$ ,  $Z$  is the proton number,  $A$  is the atomic mass, and  $r_0$  is an empirical constant  $\sim 1.2$  fm. The proton and electron number densities inside the cell are then given by

$$n_p = \frac{(p_p^F)^3}{3\pi^2} = \frac{3Z}{4\pi R_c^3} \theta(R_c - r) = \frac{3}{4\pi} \left( \frac{1}{\Delta\lambda_\pi} \right)^3 \theta(R_c - r), \quad (1.16)$$

$$n_e = \frac{(p_e^F)^3}{3\pi^2} = \frac{1}{3\pi^2} \left[ \hat{V}^2(r) + 2m_e \hat{V}(r) \right]^{3/2}, \quad (1.17)$$

$$\hat{V}(r) = eV(r) + E_e^F. \quad (1.18)$$

The Coulomb potential satisfies the Poisson equation

$$\nabla^2 V(r) = -4\pi e[n_p(r) - n_e(r)], \quad (1.19)$$

with requiring global charge neutrality of the cell enforcing the boundary conditions

$$\left. \frac{dV}{dr} \right|_{r=R_{\text{WS}}} = V(R_{\text{WS}}) = 0. \quad (1.20)$$

In practice, it is beneficial to work with dimensionless quantities, and so we define  $x = r/\lambda_\pi$  and  $\chi(r) = r\hat{V}(r)$ , such that  $x_c = R_c/\lambda_\pi$  and  $x_{\text{WS}} = R_{\text{WS}}/\lambda_\pi$ . Using these expressions results in the relativistic Thomas-Fermi equation

$$\frac{1}{3x} \frac{d^2 \chi}{dx^2} = -\frac{\alpha_{\text{EM}}}{\Delta^3} \theta(x_c - x) + \frac{4\alpha_{\text{EM}}}{9\pi} \left[ \frac{\chi^2(x)}{x^2} + 2 \frac{m_e}{m_\pi} \frac{\chi(x)}{x} \right]^{3/2}, \quad (1.21)$$

with the boundary conditions

$$\chi(0) = 0, \quad \left. \frac{d\chi}{dx} \right|_{x_{\text{WS}}} = \frac{\chi(x_{\text{WS}})}{x_{\text{WS}}}. \quad (1.22)$$

By solving these equations, we can obtain the relevant thermodynamic quantities, namely the electron and proton number densities, electron chemical potential, and the energy and pressure of the cell. The electron chemical potential is obtained by evaluating Eq. 1.15 at the cell radius, noting that the Coulomb potential must vanish there, which results in the usual expression<sup>2</sup>

$$\varepsilon_{F,e} = \sqrt{(p_e^F)^2 + m_e^2} - m_e. \quad (1.23)$$

The energy and pressure of the cell can then be obtained following the analysis presented in ref. [13]. The cell energy gains contributions from the nuclear mass, electron kinetic energy, and Coulomb interactions, such that

$$E_{\text{tot}} = M_N + E_k + E_C, \quad (1.24)$$

$$E_k = \int_0^{R_{\text{WS}}} 4\pi r^2 [\mathcal{E}_e(r) - m_e n_e(r)] dr, \quad (1.25)$$

$$E_C = \frac{1}{2} \int_{R_c}^{R_{\text{WS}}} 4\pi r^2 e [n_p(r) - n_e(r)] V(r) dr, \quad (1.26)$$

where

$$\mathcal{E}_e(r) = \frac{1}{\pi^2} \int_0^{p_e^F} p^2 \sqrt{p^2 + m_e^2} dp, \quad (1.27)$$

is the electron energy density, and  $M_N$  is the mass of the nucleus. The energy density of the cell is then simply

$$\rho_{\text{WS}} = \frac{E_{\text{tot}}}{V_{\text{WS}}}, \quad (1.28)$$

where  $V_{\text{WS}} = 4\pi R_{\text{WS}}/3$  is the volume of the WS cell. The only contribution to the internal cell pressure comes from the electrons,

$$P_e(r) = \frac{1}{3\pi^2} \int_0^{p_e^F} \frac{p^4}{\sqrt{p^2 + m_e^2}} dp, \quad (1.29)$$

with the total pressure of the cell being  $P_{\text{tot}} = P_e(R_{\text{WS}})$ . Finally, the EoS is then obtained by solving Eq. 1.21 for various cell radii, yielding a relation between  $E_{\text{tot}}$  and  $P_{\text{tot}}$  parameterised by the radius of the Wigner-Seitz cell.

---

<sup>2</sup>We use the symbol  $\varepsilon_{F,i}$  to represent the chemical potential minus the mass of a particle species  $i$ , reserving  $\mu_{F,i}$  for the full chemical potential.

EoS	WD <sub>1</sub>	WD <sub>2</sub>	WD <sub>3</sub>	WD <sub>4</sub>
$\rho_c$ [g cm <sup>-3</sup> ]	$1.47 \times 10^6$	$3.84 \times 10^7$	$3.13 \times 10^8$	$2.31 \times 10^{10}$
$M_\star$ [ $M_\odot$ ]	0.440	1.000	1.252	1.384
$R_\star$ [km]	$9.39 \times 10^3$	$5.38 \times 10^3$	$3.29 \times 10^3$	$1.25 \times 10^3$
$v_{\text{esc}}(R_\star)$ [km/s]	$3.72 \times 10^3$	$7.03 \times 10^3$	$1.01 \times 10^4$	$1.71 \times 10^4$

**Table 1.1:** Four configurations for white dwarfs composed of carbon, with an FMT EoS. Shown are the central densities,  $\rho_c$ , stellar mass  $M_\star$  and radius  $R_\star$ , and escape velocity at the edge of the WD,  $v_{\text{esc}}$ .

Different WD configurations can be obtained, assuming a non-rotating spherically symmetric star, by solving the Tolman-Oppenheimer-Volkoff (TOV) equations [7, 8] coupled to the FMT EoS with different initial conditions for the pressure at the centre of the star. In Fig. 1.1 we show radial profiles for  $n_e$  (top left),  $\mu_{F,e}$  (top right), and escape velocity  $v_{\text{esc}}$  (bottom) for the carbon WDs in Table 1.1. Note that the difference in radius between the lightest and heaviest WD in Table 1.1 spans almost one order of magnitude, while the electron number densities in the core can vary up to 4 orders of magnitude (see top left panel). As expected, electrons are more degenerate in more compact WDs and become relativistic (see top right panel). The escape velocity can reach  $\mathcal{O}(0.1 c)$  at the interior of the most compact WDs, while for very low mass WDs it can be as low as  $\sim 0.003 c$ .

The mass-radius relations obtained from a zero-temperature EoS begin to deviate from observations for low-mass WDs. To address this discrepancy, finite temperature effects can be introduced to the EoS [14]. The extension to finite temperatures is made by reintroducing the temperature dependence in the Fermi-Dirac distributions. Now, the electron chemical potential is no longer simply the Fermi energy of the system due to thermal corrections. Define the finite temperature Fermi-Dirac integrals of degree  $s$  as

$$F_s(\eta, \beta) = \int_0^\infty \frac{t^s \sqrt{1 + (\beta/2)t}}{1 + e^{t-\eta}} dt, \quad (1.30)$$

where we define the dimensionless quantities

$$t = \frac{E_e - m_e}{T_\star}, \quad (1.31)$$

$$\eta = \frac{\varepsilon_{F,e}}{T_\star}, \quad (1.32)$$

$$\beta = \frac{T_\star}{m_e}, \quad (1.33)$$

for a star at temperature  $T_\star$ . The Thomas-Fermi equilibrium condition within the

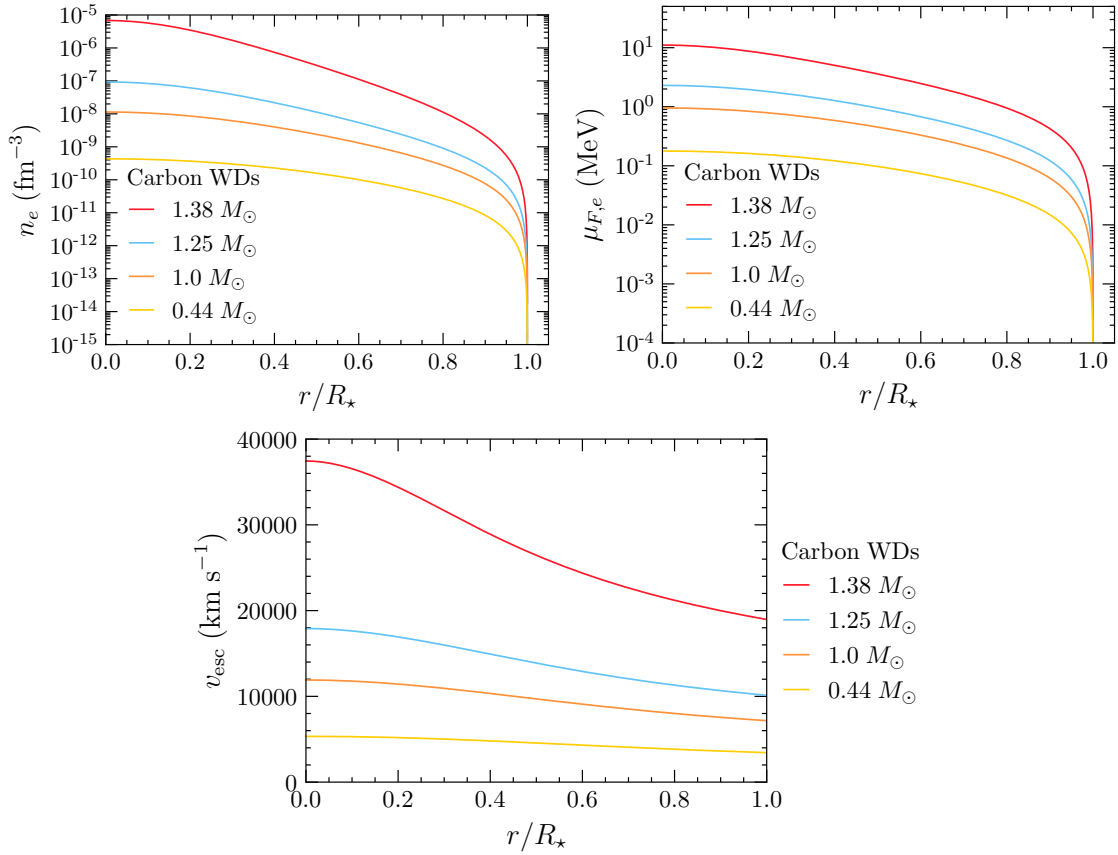


**Figure 1.1:** Electron number density (top left), chemical potential (top right), and escape velocity (bottom) radial profiles for the carbon WDs with FMT EoS in Table 1.1. The radial distance of each profile has been normalised to the radius of the star.

WS cell is now given by

$$\varepsilon_{F,e}(r) - eV(r) = T_\star \eta(r) - eV(r) = \text{constant}, \quad (1.34)$$

with the Coulpmb potential vanishing at the boundary of the cell as before. We now make the change of variables into the dimensionless quantities  $\chi/r = \varepsilon_{F,e}/(\hbar c)$  and  $x = x/x_{\text{WS}}$  so that the Poisson equation 1.19 becomes

$$\frac{d^2\chi}{dx^2} = -4\pi\alpha_{\text{EM}}x \left( \frac{3}{4\pi\Delta^3} \theta(x_c - x) - \frac{\sqrt{2}}{\pi^2} \left( \frac{m_e}{m_\pi} \right)^2 [F_{1/2}(\eta, \beta) + \beta F_{3/2}(\eta, \beta)] \right), \quad (1.35)$$

$$\eta(x) = \left( \frac{1}{\lambda_\pi T_\star} \right) \frac{\chi(x)}{x}, \quad (1.36)$$

with the same boundary conditions as in Eq. 1.22.

The total energy of the cell remains very similar to the zero-temperature case, the main differences being it gains a contribution from the thermal motion of the nucleus,

$$E_{\text{th}} = \frac{3}{2}T_{\star}, \quad (1.37)$$

and that the electron energy density is now given by

$$\mathcal{E}_e = m_e n_e + \frac{\sqrt{2}}{\pi^2} m_e^4 \beta^{5/2} [F_{3/2}(\eta, \beta) + \beta F_{5/2}(\eta, \beta)]. \quad (1.38)$$

The pressure of the cell will now gain contributions from the motion of the nucleus as well as the electron, such that the total pressure is

$$P_{\text{tot}} = P_N + P_e, \quad (1.39)$$

$$P_N = \frac{2}{3} \frac{E_{\text{th}}}{V_{\text{WS}}} = \frac{T_{\star}}{V_{\text{WS}}}, \quad (1.40)$$

$$P_e = \frac{2^{3/2}}{3\pi} m e^4 \beta^{5/2} [F_{3/2}(\eta(x_{\text{WS}}), \beta) + \beta F_{5/2}(\eta(x_{\text{WS}}), \beta)]. \quad (1.41)$$

In Fig. 1.2 we show the Mass-Radius relations obtained from the zero temperature FMT EoS together with several finite temperature configurations. As can be seen, the deviations from the zero temperature approximation begin at rather high temperatures,  $T_{\star} \gtrsim 10^7$  K, for masses  $\lesssim 0.6M_{\odot}$ . Additionally, we show observations of WDs from the Gaia early data release 2 (EDR2) report [15] as the blue dots. As mentioned above, the Mass-Radius relation seen from these observations significantly deviates from the zero temperature EoS as low masses. Note that while not represented in this figure, the temperature of the WDs increases in a similar gradient as would be expected from the FMT EoS.

Given the non-linear nature of the differential equations that describe the FMT EoS (both at zero and finite temperatures), solving the system is a numerically challenging task. As there are no publically available resources to help solve these systems, a significant amount of time was put into solving this problem. As such, we have outlined in Appendix **ADD THIS APPENDIX** the method employed in numerically solving the differential equations.

### 1.2.2 Observational Status

The rate at which the energy of the WD core is radiated away is determined by the outer non-degenerate layers. Spectroscopic observations shed light on the composition of these layers and can be used to classify WDs in terms of  $\sim$  six spectral types.

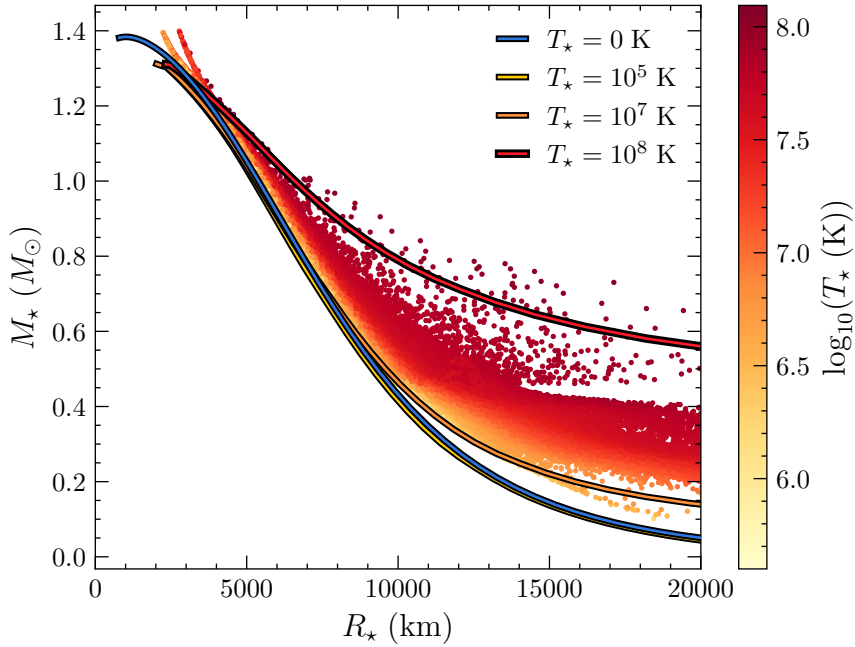


**Figure 1.2:** Mass-Radius relation of WDs calculated from the FMT EoS in the zero temperature approximation (dark blue), at  $10^5$  K (yellow),  $10^7$  K (orange), and  $10^8$  K (red), together with observed WDs from Gaia EDR2 observations [15] (light blue dots).

Most of the observed WDs lie in the DA (hydrogen-rich) and DB (helium-rich) categories. Note that as WDs slowly cool, they undergo spectral evolution. There is a well-defined relation between their luminosity and age (cooling time) that, together with recent breakthroughs in theory and observations, allow to estimate the age of the stars in the solar neighbourhood and to date the nearest star clusters [16–20].

Over the past few decades, WDs have been extensively observed using photometry and spectroscopy. Most of the WDs, spectroscopically confirmed, have been discovered by large area surveys, such as the Sloan Digital Sky Survey (SDSS) [21]. However, these local samples are dominated by young WDs with relatively high effective temperatures<sup>3</sup> ( $T_{\text{eff}} \gtrsim 10^4$  K) [22–26]. Recently, the local volume sample of nearby stars within  $\sim 100$  pc has been catalogued by the Gaia spacecraft [27, 28], an astrometric mission. New WD candidates have been identified [15], followed by dedicated spectroscopic observations [29, 30], increasing the local sample of cool WDs ( $T_{\text{eff}} \lesssim 5000$  K).

On the other hand, globular clusters (GCs) are the oldest known stellar systems

<sup>3</sup>The effective temperature is the temperature that characterises the surface of the star, assuming that WDs are perfect blackbody emitters, i.e.  $L_\gamma = 4\pi\sigma_{SB} R_*^2 T_{\text{eff}}^4$ , where  $\sigma_{SB}$  is the Stefan–Boltzmann constant.

in the Galaxy. Among them is Messier 4 (M4), also classified as NGC 6121, which is the closest globular cluster to Earth,  $\sim 1.9$  kpc away [31–33]. The age of M4, 11.6 Gyr, has been estimated using observations of faint cold WDs with the Hubble Space Telescope (HST) [16, 18]. This HST data, corrected for reddening and extinction, was converted into luminosities and effective temperatures in ref. [34]. From these calculations, it is possible to infer WD radii and their corresponding masses assuming a mass-radius relation.

We should note that there is no evidence so far that globular clusters are embedded in DM halos. Furthermore, there is no consensus on the scenario that leads to globular cluster formation. Observations and simulations suggest that there is more than one plausible mechanism. In the hierarchical structure formation scenario of standard cosmology, old, metal-poor, globular clusters are formed within their halos before or shortly after the onset of reionization [35–39]. Old globular clusters with intermediate metallicities, such as M4 [40–42], could have been accreted from small satellite galaxies and lost a large fraction of their initial DM content due to tidal stripping by the host galaxy [36, 38, 43], though a small DM fraction could have survived in the innermost region of the cluster [38, 44]. Since the cool WDs observed in M4 are located in the dense core of the globular cluster, well within the tidal radius, it is expected that the DM content in this region has survived tidal disruption. Under this assumption, it is possible to estimate the DM density as outlined in refs. [34, 45]. The DM density at the largest radius the WDs were observed (2.3 pc) was conservatively estimated to be  $\rho_\chi = 798$  (531.5) GeV cm $^{-3}$  for a contracted (uncontracted) NFW profile [34]. It is worth noting that the DM density in M4 was found to be of the order of few GeV/cm $^3$  in ref. [46]. However, the estimation in ref. [34] for M4, adopted in this work, is in good agreement with that of ref. [47] for the GC Omega Centauri (NGC 5139).

## 1.3 Neutron Stars

### Add some intro remarks

The internal structure of an NS is significantly more complicated than that of a WD. Broadly speaking, an NS can be divided into five main regions. Working from the outside in, these are:

### Atmosphere

The atmosphere is an extremely thin layer of plasma that makes up less than 1% of the NS mass. However, it plays an extremely important role as the observed

spectrum radiation emitted by the star must pass through this star. This radiation contains valuable information about various properties of the star.

### Outer Crust

The outer crust is the thin layer of ionized Iron-56 nuclei that extends down until the density reaches the neutron drip point,  $\rho_* = \rho_{\text{ND}} \sim 4.3 \times 10^{11} \text{ g cm}^{-3}$ . This is the density at which neutrons begin to drip from the nuclei as their chemical potentials approach zero. The ionized electrons form a non-relativistic but degenerate gas, with their chemical potentials increasing as the density increases. This leads to the “neutronisation” of the nuclei as the beta-capture of electrons by protons increases.

### Inner Crust

The density within the inner crust spans the range between  $\rho_{\text{ND}} \lesssim \rho_* \lesssim 0.5\rho_0$ , with  $\rho_0 \sim 2.8 \times 10^{14} \text{ g cm}^{-3}$  the nuclear saturation density (i.e. the density of nuclear matter). Here, the neutrons that have dripped from the nuclei will potentially form a superfluid. Towards the crust-core boundary, the nuclear lattice begins taking on interesting topological structures that are distinguished by the configuration of the voids in the lattice. These are known as the so-called *pasta phases* of nuclear matter:

- 2D void cylinders creating spaghetti structures of nuclei
- Planar voids with slabs of nuclei forming lasagna sheets
- 3D cylindrical voids leading to thin 2D cylinders of nuclear ziti
- 3D spherical voids enclosed by ravioli
- 2D circular voids in sheets of Swiss cheese

Eventually, the nuclear matter becomes a uniform medium<sup>4</sup>.

### Outer Core

Once densities go above  $0.5\rho_0$ , the nuclear clusters will dissolve into a homogenous fluid that is composed of neutrons, protons, electrons, and muons known as *npeu* matter. The relative abundances of the species,  $Y_i = n_i/n_b$ , are dictated by the

---

<sup>4</sup>The nuclear marinara sauce, if you will

conditions of electrical neutrality and beta-equilibrium. Charge neutrality dictates that the abundances of the charged particles obeys

$$Y_p = Y_e + Y_\mu, \quad (1.42)$$

while beta-equilibrium refers to the balance between the weak decays of neutrons and the electron/muon capture by the protons,



with  $\ell = e, \mu$ . Muons will begin to replace electrons in these reactions once the electron chemical potential exceeds the mass of the muon,  $\mu_{F,e} \gtrsim m_\mu = 105.7 \text{ MeV}$ . As the species are all degenerate, muons cannot decay into electrons, imposing the constraint

$$\mu_{F,e} = \mu_{F,\mu}, \quad (1.45)$$

on the chemical potentials. The outer core region ends once the density reaches  $\rho_* \sim 2\rho_0$ , and we transition into the inner core.

## Inner Core

The densities within the inner cores of NSs extend between  $2\rho_0 \lesssim \rho_* \lesssim (10 - 15)\rho_0$  and are hence a mystery to this day. As the density exceeds well above any material that can be produced in a laboratory, the exact composition of this region is unknown and depends on the equation of state one adopts to describe it. Some of the more well-known candidates are

- The appearance of hyperonic matter, i.e. nucleons containing a valence strange quark. These appear once the neutron chemical potential equals the  $\Lambda^0$  hyperon, with the  $\Xi^-$  appearing once its chemical potential equals the sum of the chemical potentials of the neutrons and electrons.
- Pion/Kaon condensates. These are Bose-Einstein condensates of pion/kaon-like excitations, with the kaon also containing a valence strange quark.
- A quark-gluon plasma comprised of deconfined quarks ( $u, d$  and  $s$ ) and gluons.

### 1.3.1 Observational Status

Unlike the WDs discussed above, there are much fewer NS observations that constrain the EoS. However, recent years have seen significant strides in furthering our understanding of matter at super-nuclear densities, both from a theory and observational standpoint. On the theoretical side, these advances come from developments in chiral EFT allowing more detailed modelling of nuclear interactions [48–50], while the observational data has been bolstered thanks to the onset of gravitational wave astronomy due to the LIGO-VIRGO experiment [51–53] and the launch of the Neutron star Interior Composition Explorer (NICER) X-ray timing instrument.

Ultimately, what is needed to further constrain the NS EoS are more precise observations of NS masses and radii, which can be obtained from various observational techniques. NS masses have historically been much easier to measure than their radii. In particular, masses of NSs in binary systems can be precisely determined as the underlying gravitational theories are well-understood today [54–58]. The radii must be determined by assuming the NSs emit a blackbody spectrum, however, this method is only reliable for cool NSs where the atmospheric models are well understood [58].

The NICER experiment can provide much more precise measurements of NS radii than previous methods. This is achieved by measuring the X-ray pulse profiles of pulsars, that are sensitive to how light bends around the star. This provides information on the compactness of the star,  $GM_\star/R_\star c^2$ , that can be used to determine  $M_\star$  and  $R_\star$  given that the mass can usually be determined through other means. The heaviest NS observed to date, the millisecond pulsar PSR J0740+6620 [59, 60], had its mass determined by measuring the relativistic Shapiro time delay [61]<sup>5</sup> of the radio signal, allowing the radius to be obtained once the compactness was measured [62]. Refined analyses result in a mass of  $2.08 \pm 0.07 M_\odot$  [63] and a radius of  $12.39^{+1.30}_{-0.98}$  km [60] or  $13.71^{+2.61}_{-1.50}$  km [59] at 68% confidence levels.

Gravitational wave astronomy offers an alternative and independent determination of NS masses and radii to the electromagnetic observations above. The best candidate events for this analysis are NS binary mergers, though these are expected to be an uncommon occurrence. As the NSs inspiral toward each other, they will begin to deform due to the tidal forces they induce on one another [64]. This deformation will alter the waveform observed at the detectors, with the shift in the phase of the waveform depending on the mass ratio,  $q = M_2/M_1 < 1$ , the chirp mass of the system,  $\mathcal{M}_{\text{chirp}} = (M_1 M_2)^{3/5}/(M_1 + M_2)^{1/5}$ , and a combination of the tidal deformabilities,  $\bar{\Lambda}$ . The latter refers to how susceptible the star is to deformation due to tidal forces acting upon it, with larger values corresponding to

---

<sup>5</sup>This refers to the time it takes for light to move out of a gravitational well taking longer than the naive Newtonian prediction due to the curvature of space-time.

less compact objects. Comparing the observed waveform to that determined from precise numerical simulations allows constraints to be placed on these parameters, and ultimately on the masses and radii of the merging NSs.

Furthermore, the electromagnetic emission from the remnant object provides information about the maximum mass an NS can achieve. If the mass of the remnant object is too large, it will collapse into a black hole, and it is highly unlikely that a gamma-ray burst will occur. If the remnant does not immediately collapse, then its mass and how it is rotating determines whether it will be hydrodynamically stable, unstable, or metastable against gravitational collapse. A remnant that undergoes differential rotation<sup>6</sup> can support heavier masses than one that is uniformly rotating. Hence, the afterglow spectrum can inform us as to how the star is rotating. Comparing the maximum mass supported by this rotation to the initial mass after inspiral yields an upper bound on the maximum NS mass achievable.

To date, the only confirmed NS-NS merger is the merger event GW170817 observed at LIGO-VIRGO in 2017 [52, 53], with the gamma-ray burst counterpart signal observed at the Fermi Gamma-ray Burst Monitor and INTEGRAL satellite [51]. These observations led to the constraint that the radius of a  $1.4M_{\odot}$  NS has an upper bound of  $R_{1.4} < 13.3$  km [65, 66], and that the maximum NS mass must be  $M_{\text{NS,MAX}} < 2.18M_{\odot}$  [51].

### 1.3.2 Choices of Neutron Star Equation of State

Given the scarce constraints that have been placed on the NS mass-radius relation, there are numerous equations of state in the literature that can be used to incorporate the internal structure into our calculations. In this work, we adopt two different EoSs, which we detail here.

#### The Brussels-Montreal EoS

The first family of EoSs adopted in this work are based on the Brussels-Montreal (BSk) energy density functionals [67–72], for cold, non-accreting NSs. In these models, the density-dependent nucleon interactions are accounted for via a mean-field approximation in either the Hartree-Fock (HF) or Hartree-Fock-Bogoliubov (HFB) formalism<sup>7</sup>, through effective Skyrme type forces [73, 74]. The BSk EoS family are unified EoSs, meaning they describe all the regions of the NS interior using the single effective Hamiltonian.

---

<sup>6</sup>This is when components of the star at different latitudes have different angular velocities.

<sup>7</sup>The HF method accounts for the energy associated with nucleon pairings, while the HFB method neglects this contribution.

These EoSs are minimal in the sense that they only account for  $npe\mu$  matter, not incorporating any exotic species within the NS core. Additionally, the Skyrme forces that describe the nuclear interaction are treated non-relativistically, while the nucleons in heavier stars become can become semi-relativistic.



# Definition of Symbols and Abbreviations

**$C_{\text{geo}}$**  Geometric Capture Rate

**DM** Dark Matter

**$K_\chi$**  Dark Matter Kinetic Energy

$\rho_\chi$  DM halo density

**$m_\chi$**  Dark Matter Mass

**EFT** Effective Field Theory

**EoS** Equation of State

**$f_{\text{FD}}$**  Fermi-Dirac Distribution

$\epsilon_{F,i}$  Fermi kinetic energy of target species

$|\overline{\mathcal{M}}|^2$  Spin-averaged squared matrix element

**$\mu$**  DM-Target mass ratio,  $m_\chi/m_i$

**NS** Neutron Star

**PB** Pauli Blocking

**QMC** Quark-Meson-Coupling EoS

$\sigma_{\text{th}}$  Threshold Cross Section

**$T_{\text{eq}}$**  Equilibrium Temperature

**$t_{\text{eq}}$**  Capture-Accretion equilibrium time

**$T_\star$**  Temperature of the star

**$t_{\text{therm}}$**  Thermalisation time

**$v_d$**  DM halo dispersion velocity

**$v_\star$**  Star velocity



# Bibliography

- [1] Nicole F. Bell et al. “Improved Treatment of Dark Matter Capture in Neutron Stars”. In: *JCAP* 09 (Sept. 15, 2020), p. 028. doi: [10.1088/1475-7516/2020/09/028](https://doi.org/10.1088/1475-7516/2020/09/028). arXiv: [2004.14888 \[hep-ph\]](https://arxiv.org/abs/2004.14888).
- [2] Nicole F. Bell et al. “Improved Treatment of Dark Matter Capture in Neutron Stars II: Leptonic Targets”. In: *JCAP* 03 (Mar. 26, 2021), p. 086. doi: [10.1088/1475-7516/2021/03/086](https://doi.org/10.1088/1475-7516/2021/03/086). arXiv: [2010.13257 \[hep-ph\]](https://arxiv.org/abs/2010.13257).
- [3] Nicole F. Bell et al. “Nucleon Structure and Strong Interactions in Dark Matter Capture in Neutron Stars”. In: *Phys. Rev. Lett.* 127.11 (Sept. 10, 2021), p. 111803. doi: [10.1103/PhysRevLett.127.111803](https://doi.org/10.1103/PhysRevLett.127.111803). arXiv: [2012.08918 \[hep-ph\]](https://arxiv.org/abs/2012.08918).
- [4] Nicole F. Bell et al. “Improved Treatment of Dark Matter Capture in White Dwarfs”. In: *JCAP* 10 (Oct. 29, 2021), p. 083. doi: [10.1088/1475-7516/2021/10/083](https://doi.org/10.1088/1475-7516/2021/10/083). arXiv: [2104.14367 \[hep-ph\]](https://arxiv.org/abs/2104.14367).
- [5] Filippo Anzuini et al. “Improved Treatment of Dark Matter Capture in Neutron Stars III: Nucleon and Exotic Targets”. In: *JCAP* 11.11 (Nov. 29, 2021), p. 056. doi: [10.1088/1475-7516/2021/11/056](https://doi.org/10.1088/1475-7516/2021/11/056). arXiv: [2108.02525 \[hep-ph\]](https://arxiv.org/abs/2108.02525).
- [6] Nicole F. Bell et al. “Thermalization and Annihilation of Dark Matter in Neutron Stars”. In: *arXiv:2312.11892 [hep-ph]* (Dec. 2023). arXiv: [2312.11892 \[hep-ph\]](https://arxiv.org/abs/2312.11892).
- [7] Richard C. Tolman. “Static Solutions of Einstein’s Field Equations for Spheres of Fluid”. In: *Physical Review* 55.4 (1939), pp. 364–373. doi: [10.1103/PhysRev.55.364](https://doi.org/10.1103/PhysRev.55.364).
- [8] J. R. Oppenheimer and G. M. Volkoff. “On Massive Neutron Cores”. In: *Physical Review* 55.4 (1939), pp. 374–381. doi: [10.1103/PhysRev.55.374](https://doi.org/10.1103/PhysRev.55.374).
- [9] G. Fontaine, P. Brassard, and P. Bergeron. “The Potential of White Dwarf Cosmochronology”. In: *Publications of the Astronomical Society of the Pacific* 113.782 (Apr. 2001), pp. 409–435. doi: [10.1086/319535](https://doi.org/10.1086/319535).
- [10] E. E. Salpeter. “Energy and Pressure of a Zero-Temperature Plasma.” In: *Astrophysical Journal* 134 (Nov. 1961), p. 669. doi: [10.1086/147194](https://doi.org/10.1086/147194).

- [11] R.P. Feynman, N. Metropolis, and E. Teller. “Equations of State of Elements Based on the Generalized Fermi-Thomas Theory”. In: *Physical Review* 75 (1949), pp. 1561–1573. DOI: [10.1103/PhysRev.75.1561](https://doi.org/10.1103/PhysRev.75.1561).
- [12] M. Rotondo et al. “On the Relativistic Thomas-Fermi Treatment of Compressed Atoms and Compressed Nuclear Matter Cores of Stellar Dimensions”. In: *Physical Review C: Nuclear Physics* 83 (2011), p. 045805. DOI: [10.1103/PhysRevC.83.045805](https://doi.org/10.1103/PhysRevC.83.045805). arXiv: [0911.4622 \[astro-ph.SR\]](https://arxiv.org/abs/0911.4622).
- [13] Michael Rotondo et al. “The Relativistic Feynman-Metropolis-Teller Theory for White Dwarfs in General Relativity”. In: *Phys. Rev. D* 84 (2011), p. 084007. DOI: [10.1103/PhysRevD.84.084007](https://doi.org/10.1103/PhysRevD.84.084007). arXiv: [1012.0154 \[astro-ph.SR\]](https://arxiv.org/abs/1012.0154).
- [14] S.M. de Carvalho et al. “Relativistic Feynman-Metropolis-Teller Treatment at Finite Temperatures”. In: *Int. J. Mod. Phys. Conf. Ser.* 23 (2013), p. 244. DOI: [10.1103/PhysRevC.89.015801](https://doi.org/10.1103/PhysRevC.89.015801). arXiv: [1312.2434 \[astro-ph.SR\]](https://arxiv.org/abs/1312.2434).
- [15] Nicola Pietro Gentile Fusillo et al. “A Gaia Data Release 2 Catalogue of White Dwarfs and a Comparison with SDSS”. In: *Mon. Not. Roy. Astron. Soc.* 482.4 (Feb. 2019), pp. 4570–4591. DOI: [10.1093/mnras/sty3016](https://doi.org/10.1093/mnras/sty3016). arXiv: [1807.03315 \[astro-ph.SR\]](https://arxiv.org/abs/1807.03315).
- [16] Brad M.S. Hansen et al. “HST Observations of the White Dwarf Cooling Sequence of M4”. In: *Astrophys. J. Suppl.* 155 (2004), p. 551. DOI: [10.1086/424832](https://doi.org/10.1086/424832). arXiv: [astro-ph/0401443](https://arxiv.org/abs/astro-ph/0401443).
- [17] Brad M.S. Hansen et al. “The White Dwarf Cooling Sequence of NGC 6397”. In: *Astrophysical Journal* 671 (2007), p. 380. DOI: [10.1086/522567](https://doi.org/10.1086/522567). arXiv: [astro-ph/0701738](https://arxiv.org/abs/astro-ph/0701738).
- [18] Luigi R. Bedin et al. “The End of the White Dwarf Cooling Sequence in M4: An Efficient Approach”. In: *Astrophysical Journal* 697.2 (June 2009), pp. 965–979. DOI: [10.1088/0004-637X/697/2/965](https://doi.org/10.1088/0004-637X/697/2/965). arXiv: [0903.2839 \[astro-ph.GA\]](https://arxiv.org/abs/0903.2839).
- [19] B. M. S. Hansen et al. “An Age Difference of Two Billion Years between a Metal-Rich and a Metal-Poor Globular Cluster”. In: *Nature* 500.7460 (Aug. 2013), pp. 51–53. DOI: [10.1038/nature12334](https://doi.org/10.1038/nature12334). arXiv: [1308.0032 \[astro-ph.SR\]](https://arxiv.org/abs/1308.0032).
- [20] Mukremin Kilic et al. “The Ages of the Thin Disk, Thick Disk, and the Halo from Nearby White Dwarfs”. In: *Astrophysical Journal* 837.162 (2 Mar. 2017), p. 162. DOI: [10.3847/1538-4357/aa62a5](https://doi.org/10.3847/1538-4357/aa62a5). arXiv: [1702.06984 \[astro-ph.SR\]](https://arxiv.org/abs/1702.06984).
- [21] Donald G. York et al. “The Sloan Digital Sky Survey: Technical Summary”. In: *Astronomy Journal* 120.FERMILAB-PUB-01-319-A (2000), pp. 1579–1587. DOI: [10.1086/301513](https://doi.org/10.1086/301513). arXiv: [astro-ph/0006396](https://arxiv.org/abs/astro-ph/0006396).

- [22] Daniel J. Eisenstein et al. “A Catalog of Spectroscopically Confirmed White Dwarfs from the Sloan Digital Sky Survey Data Release 4”. In: *Astrophys. J. Suppl.* 167.FERMILAB-PUB-06-603-A (2006), pp. 40–58. doi: [10.1086/507110](https://doi.org/10.1086/507110). arXiv: [astro-ph/0606700](https://arxiv.org/abs/astro-ph/0606700).
- [23] S. J. Kleinman et al. “SDSS DR7 White Dwarf Catalog”. In: *Astrophys. J. Suppl.* 204.5 (1 Jan. 2013), p. 5. doi: [10.1088/0067-0049/204/1/5](https://doi.org/10.1088/0067-0049/204/1/5). arXiv: [1212.1222 \[astro-ph.SR\]](https://arxiv.org/abs/1212.1222).
- [24] P. -E. Tremblay et al. “The Field White Dwarf Mass Distribution”. In: *Mon. Not. Roy. Astron. Soc.* 461.2 (Sept. 2016), pp. 2100–2114. doi: [10.1093/mnras/stw1447](https://doi.org/10.1093/mnras/stw1447). arXiv: [1606.05292 \[astro-ph.SR\]](https://arxiv.org/abs/1606.05292).
- [25] S. O. Kepler et al. “White Dwarf Mass Distribution”. In: *20th European White Dwarf Workshop*. Ed. by P. -E. Tremblay, B. Gaensicke, and T. Marsh. Vol. 509. Astronomical Society of the Pacific Conference Series. Mar. 2017, p. 421. arXiv: [1610.00371 \[astro-ph.SR\]](https://arxiv.org/abs/1610.00371).
- [26] S. O. Kepler et al. “White Dwarf and Subdwarf Stars in the Sloan Digital Sky Survey Data Release 14”. In: *Monthly Notices of the Royal Astronomical Society* 486.2 (June 2019), pp. 2169–2183. doi: [10.1093/mnras/stz960](https://doi.org/10.1093/mnras/stz960). arXiv: [1904.01626 \[astro-ph.SR\]](https://arxiv.org/abs/1904.01626).
- [27] C. Babusiaux et al. “Gaia Data Release 2. Observational Hertzsprung-Russell Diagrams”. In: *Astronomy and Astrophysics* 616.A10 (Aug. 2018), A10. doi: [10.1051/0004-6361/201832843](https://doi.org/10.1051/0004-6361/201832843). arXiv: [1804.09378 \[astro-ph.SR\]](https://arxiv.org/abs/1804.09378).
- [28] R. L. Smart et al. “Gaia Early Data Release 3. The Gaia Catalogue of Nearby Stars”. In: *Astron. Astrophys.* 649.A6 (May 2021), A6. doi: [10.1051/0004-6361/202039498](https://doi.org/10.1051/0004-6361/202039498). arXiv: [2012.02061 \[astro-ph.SR\]](https://arxiv.org/abs/2012.02061).
- [29] P. -E. Tremblay et al. “Gaia White Dwarfs within 40 Pc - I. Spectroscopic Observations of New Candidates”. In: *Mon. Not. Roy. Astron. Soc.* 497.1 (July 2020), pp. 130–145. doi: [10.1093/mnras/staa1892](https://doi.org/10.1093/mnras/staa1892). arXiv: [2006.00965 \[astro-ph.SR\]](https://arxiv.org/abs/2006.00965).
- [30] Jack McCleery et al. “Gaia White Dwarfs within 40 Pc II: The Volume-Limited Northern Hemisphere Sample”. In: *Mon. Not. Roy. Astron. Soc.* 499.2 (July 2020), pp. 1890–1908. doi: [10.1093/mnras/staa2030](https://doi.org/10.1093/mnras/staa2030). arXiv: [2006.00874 \[astro-ph.SR\]](https://arxiv.org/abs/2006.00874).
- [31] J. R. Neeley et al. “On the Distance of the Globular Cluster M4 (NGC 6121) Using RR Lyrae Stars. II. Mid-infrared Period-Luminosity Relations.” In: *Astrophysical Journal* 808.11 (1 July 2015), p. 11. doi: [10.1088/0004-637X/808/1/11](https://doi.org/10.1088/0004-637X/808/1/11). arXiv: [1505.07858 \[astro-ph.SR\]](https://arxiv.org/abs/1505.07858).

- [32] Laura L. Watkins and Roeland P. van der Marel. “Tycho-Gaia Astrometric Solution Parallaxes and Proper Motions for Five Galactic Globular Clusters”. In: *Astrophysical Journal* 839.89 (2 Apr. 2017), p. 89. doi: [10.3847/1538-4357/aa696f](https://doi.org/10.3847/1538-4357/aa696f). arXiv: [1611.03170 \[astro-ph.SR\]](https://arxiv.org/abs/1611.03170).
- [33] Zhengyi Shao and Lu Li. “Gaia Parallax of Milky Way Globular Clusters - A Solution of Mixture Model”. In: *Mon. Not. Roy. Astron. Soc.* 489.3 (Nov. 2019), pp. 3093–3101. doi: [10.1093/mnras/stz2317](https://doi.org/10.1093/mnras/stz2317). arXiv: [1908.06031 \[astro-ph.GA\]](https://arxiv.org/abs/1908.06031).
- [34] Matthew McCullough and Malcolm Fairbairn. “Capture of Inelastic Dark Matter in White Dwarves”. In: *Physical Review D* 81.8 (2010), p. 083520. doi: [10.1103/PhysRevD.81.083520](https://doi.org/10.1103/PhysRevD.81.083520). arXiv: [1001.2737 \[hep-ph\]](https://arxiv.org/abs/1001.2737).
- [35] P. J. E. Peebles. “Dark Matter and the Origin of Galaxies and Globular Star Clusters”. In: *Astrophysical Journal* 277 (Feb. 1984), pp. 470–477. doi: [10.1086/161714](https://doi.org/10.1086/161714).
- [36] Volker Bromm and Catherine J. Clarke. “The Formation of the First Globular Clusters in Dwarf Galaxies before the Epoch of Reionization”. In: *Astrophysical Journal, Letters to the Editor* 566 (2002), p. L1. doi: [10.1086/339440](https://doi.org/10.1086/339440). arXiv: [astro-ph/0201066](https://arxiv.org/abs/astro-ph/0201066).
- [37] Sergey Mashchenko and Alison Sills. “Globular Clusters with Dark Matter Halos. 1. Initial Relaxation”. In: *Astrophysical Journal* 619 (2005), p. 243. doi: [10.1086/426132](https://doi.org/10.1086/426132). arXiv: [astro-ph/0409605](https://arxiv.org/abs/astro-ph/0409605).
- [38] Sergey Mashchenko and Alison Sills. “Globular Clusters with Dark Matter Halos. 2. Evolution in Tidal Field”. In: *Astrophysical Journal* 619 (2005), p. 258. doi: [10.1086/426133](https://doi.org/10.1086/426133). arXiv: [astro-ph/0409606](https://arxiv.org/abs/astro-ph/0409606).
- [39] Massimo Ricotti, Owen H. Parry, and Nickolay Y. Gnedin. “A Common Origin for Globular Clusters and Ultra-Faint Dwarfs in Simulations of the First Galaxies”. In: *Astrophysical Journal* 831.FERMILAB-PUB-16-286-A (2 2016), p. 204. doi: [10.3847/0004-637X/831/2/204](https://doi.org/10.3847/0004-637X/831/2/204). arXiv: [1607.04291 \[astro-ph.GA\]](https://arxiv.org/abs/1607.04291).
- [40] E. Carretta et al. “Na-O Anticorrelation and HB. VII. The Chemical Composition of First and Second-Generation Stars in 15 Globular Clusters from GIRAFFE Spectra”. In: *Astronomy and Astrophysics* 505.1 (Oct. 2009), pp. 117–138. doi: [10.1051/0004-6361/200912096](https://doi.org/10.1051/0004-6361/200912096). arXiv: [0909.2938 \[astro-ph.GA\]](https://arxiv.org/abs/0909.2938).
- [41] E. Carretta et al. “Na-O Anticorrelation and HB. VIII. Proton-capture Elements and Metallicities in 17 Globular Clusters from UVES Spectra”. In: *Astronomy and Astrophysics* 505.1 (Oct. 2009), pp. 139–155. doi: [10.1051/0004-6361/200912097](https://doi.org/10.1051/0004-6361/200912097). arXiv: [0909.2941 \[astro-ph.GA\]](https://arxiv.org/abs/0909.2941).

- [42] Y. Wang et al. “Sodium Abundances of AGB and RGB Stars in Galactic Globular Clusters. II. Analysis and Results of NGC 104, NGC 6121, and NGC 6809”. In: *Astronomy and Astrophysics* 607.A135 (Nov. 2017), A135. DOI: [10.1051/0004-6361/201730976](https://doi.org/10.1051/0004-6361/201730976). arXiv: [1708.07634 \[astro-ph.SR\]](https://arxiv.org/abs/1708.07634).
- [43] Takayuki R. Saitoh et al. “Tidal Disruption of Dark Matter Halos around Proto-Globular Clusters”. In: *Astrophysical Journal* 640 (2006), pp. 22–30. DOI: [10.1086/500104](https://doi.org/10.1086/500104). arXiv: [astro-ph/0511692](https://arxiv.org/abs/astro-ph/0511692).
- [44] Rodrigo Ibata et al. “Do Globular Clusters Possess Dark Matter Halos? A Case Study in NGC 2419”. In: *Mon. Not. Roy. Astron. Soc.* 428 (2013), p. 3648. DOI: [10.1093/mnras/sts302](https://doi.org/10.1093/mnras/sts302). arXiv: [1210.7787 \[astro-ph.CO\]](https://arxiv.org/abs/1210.7787).
- [45] Gianfranco Bertone and Malcolm Fairbairn. “Compact Stars as Dark Matter Probes”. In: *Physical Review D* 77.4 (2008), p. 043515. DOI: [10.1103/PhysRevD.77.043515](https://doi.org/10.1103/PhysRevD.77.043515). arXiv: [0709.1485 \[astro-ph\]](https://arxiv.org/abs/0709.1485).
- [46] Dan Hooper et al. “Inelastic Dark Matter As An Efficient Fuel For Compact Stars”. In: *Physical Review D* 81.10 (2010), p. 103531. DOI: [10.1103/PhysRevD.81.103531](https://doi.org/10.1103/PhysRevD.81.103531). arXiv: [1002.0005 \[hep-ph\]](https://arxiv.org/abs/1002.0005).
- [47] Pau Amaro-Seoane et al. “Probing Dark Matter Crests with White Dwarfs and IMBHs”. In: *Monthly Notices of the Royal Astronomical Society* 459.1 (June 11, 2016), pp. 695–700. DOI: [10.1093/mnras/stw433](https://doi.org/10.1093/mnras/stw433). arXiv: [1512.00456 \[astro-ph.CO\]](https://arxiv.org/abs/1512.00456).
- [48] K. Hebeler and A. Schwenk. “Chiral Three-Nucleon Forces and Neutron Matter”. In: *Physical Review C* 82.1 (2010), p. 014314. DOI: [10.1103/PhysRevC.82.014314](https://doi.org/10.1103/PhysRevC.82.014314). arXiv: [0911.0483 \[nucl-th\]](https://arxiv.org/abs/0911.0483).
- [49] I. Tews et al. “Neutron Matter at Next-to-Next-to-Next-to-Leading Order in Chiral Effective Field Theory”. In: *Physical Review Letters* 110.3 (Jan. 15, 2013), p. 032504. DOI: [10.1103/PhysRevLett.110.032504](https://doi.org/10.1103/PhysRevLett.110.032504). arXiv: [1206.0025 \[nucl-th\]](https://arxiv.org/abs/1206.0025).
- [50] Ingo Tews et al. “Constraining the Speed of Sound inside Neutron Stars with Chiral Effective Field Theory Interactions and Observations”. In: *The Astrophysical Journal* 860.2 (June 21, 2018), p. 149. DOI: [10.3847/1538-4357/aac267](https://doi.org/10.3847/1538-4357/aac267). arXiv: [1801.01923 \[nucl-th\]](https://arxiv.org/abs/1801.01923).
- [51] B. P. Abbott et al. “Gravitational Waves and Gamma-Rays from a Binary Neutron Star Merger: GW170817 and GRB 170817A”. In: *Astrophysical Journal* 848.LIGO-P1700308 (2 2017), p. L13. DOI: [10.3847/2041-8213/aa920c](https://doi.org/10.3847/2041-8213/aa920c). arXiv: [1710.05834 \[astro-ph.HE\]](https://arxiv.org/abs/1710.05834).

- [52] B.P. Abbott, R. Abbott, T.D. Abbott, et al. “GW170817: Measurements of Neutron Star Radii and Equation of State”. In: *Physical Review Letters* 121.16 (Oct. 16, 2018), p. 161101. DOI: [10.1103/PhysRevLett.121.161101](https://doi.org/10.1103/PhysRevLett.121.161101). arXiv: [1805.11581 \[gr-qc\]](https://arxiv.org/abs/1805.11581).
- [53] B. P. Abbott et al. “Properties of the Binary Neutron Star Merger GW170817”. In: *Physical Review X* 9.1 (2019), p. 011001. DOI: [10.1103/PhysRevX.9.011001](https://doi.org/10.1103/PhysRevX.9.011001). arXiv: [1805.11579 \[gr-qc\]](https://arxiv.org/abs/1805.11579).
- [54] Andrew W. Steiner, James M. Lattimer, and Edward F. Brown. “The Equation of State from Observed Masses and Radii of Neutron Stars”. In: *The Astrophysical Journal* 722.1 (2010), pp. 33–54. DOI: [10.1088/0004-637X/722/1/33](https://doi.org/10.1088/0004-637X/722/1/33). arXiv: [1005.0811 \[astro-ph.HE\]](https://arxiv.org/abs/1005.0811).
- [55] James M. Lattimer and Andrew W. Steiner. “Neutron Star Masses and Radii from Quiescent Low-Mass X-ray Binaries”. In: *The Astrophysical Journal* 784.2 (Mar. 14, 2014), p. 123. DOI: [10.1088/0004-637X/784/2/123](https://doi.org/10.1088/0004-637X/784/2/123). arXiv: [1305.3242 \[astro-ph.HE\]](https://arxiv.org/abs/1305.3242).
- [56] Feryal Ozel et al. “The Dense Matter Equation of State from Neutron Star Radius and Mass Measurements”. In: *The Astrophysical Journal* 820.1 (Mar. 15, 2016), p. 28. DOI: [10.3847/0004-637X/820/1/28](https://doi.org/10.3847/0004-637X/820/1/28). arXiv: [1505.05155 \[astro-ph.HE\]](https://arxiv.org/abs/1505.05155).
- [57] Feryal Özel and Paulo Freire. “Masses, Radii, and the Equation of State of Neutron Stars”. In: *Ann. Rev. Astron. Astrophys.* 54 (July 27, 2016), pp. 401–440. DOI: [10.1146/annurev-astro-081915-023322](https://doi.org/10.1146/annurev-astro-081915-023322). arXiv: [1603.02698 \[astro-ph.HE\]](https://arxiv.org/abs/1603.02698).
- [58] M. Coleman Miller and Frederick K. Lamb. “Observational Constraints on Neutron Star Masses and Radii”. In: *The European Physical Journal A* 52.3 (Mar. 22, 2016), p. 63. DOI: [10.1140/epja/i2016-16063-8](https://doi.org/10.1140/epja/i2016-16063-8). arXiv: [1604.03894 \[astro-ph.HE\]](https://arxiv.org/abs/1604.03894).
- [59] M. C. Miller et al. “The Radius of PSR J0740+6620 from NICER and XMM-Newton Data”. In: *The Astrophysical Journal Letters* 918.2 (Sept. 8, 2021), p. L28. DOI: [10.3847/2041-8213/ac089b](https://doi.org/10.3847/2041-8213/ac089b). arXiv: [2105.06979 \[astro-ph.HE\]](https://arxiv.org/abs/2105.06979).
- [60] Thomas E. Riley et al. “A NICER View of the Massive Pulsar PSR J0740+6620 Informed by Radio Timing and XMM-Newton Spectroscopy”. In: *The Astrophysical Journal Letters* 918.2 (Sept. 8, 2021), p. L27. DOI: [10.3847/2041-8213/ac0a81](https://doi.org/10.3847/2041-8213/ac0a81). arXiv: [2105.06980 \[astro-ph.HE\]](https://arxiv.org/abs/2105.06980).
- [61] Irwin I. Shapiro. “Fourth Test of General Relativity”. In: *Physical Review Letters* 13.26 (1964), pp. 789–791. DOI: [10.1103/PhysRevLett.13.789](https://doi.org/10.1103/PhysRevLett.13.789).

- [62] H. T. Cromartie et al. “Relativistic Shapiro Delay Measurements of an Extremely Massive Millisecond Pulsar”. In: *Nature Astronomy* 4.1 (Sept. 16, 2019), pp. 72–76. DOI: [10.1038/s41550-019-0880-2](https://doi.org/10.1038/s41550-019-0880-2). arXiv: [1904.06759 \[astro-ph.HE\]](https://arxiv.org/abs/1904.06759).
- [63] Emmanuel Fonseca et al. “Refined Mass and Geometric Measurements of the High-Mass PSR J0740+6620”. In: *The Astrophysical Journal Letters* 915.1 (July 1, 2021), p. L12. DOI: [10.3847/2041-8213/ac03b8](https://doi.org/10.3847/2041-8213/ac03b8). arXiv: [2104.00880 \[astro-ph.HE\]](https://arxiv.org/abs/2104.00880).
- [64] James M. Lattimer. “Neutron Star Mass and Radius Measurements”. In: *Universe* 5.7 (June 28, 2019), p. 159. DOI: [10.3390/universe5070159](https://doi.org/10.3390/universe5070159).
- [65] B. P. Abbott et al. “GW170817: Measurements of Neutron Star Radii and Equation of State”. In: *Physical Review Letters* 121.16 (Oct. 16, 2018), p. 161101. DOI: [10.1103/PhysRevLett.121.161101](https://doi.org/10.1103/PhysRevLett.121.161101). arXiv: [1805.11581 \[gr-qc\]](https://arxiv.org/abs/1805.11581).
- [66] Soumi De et al. “Tidal Deformabilities and Radii of Neutron Stars from the Observation of GW170817”. In: *Physical Review Letters* 121.9 (Aug. 29, 2018), p. 091102. DOI: [10.1103/PhysRevLett.121.091102](https://doi.org/10.1103/PhysRevLett.121.091102). arXiv: [1804.08583 \[astro-ph.HE\]](https://arxiv.org/abs/1804.08583).
- [67] N. Chamel, S. Goriely, and J.M. Pearson. “Further Explorations of Skyrme-Hartree-Fock-Bogoliubov Mass Formulas. XI. Stabilizing Neutron Stars against a Ferromagnetic Collapse”. In: *Physical Review C: Nuclear Physics* 80 (2009), p. 065804. DOI: [10.1103/PhysRevC.80.065804](https://doi.org/10.1103/PhysRevC.80.065804). arXiv: [0911.3346 \[nucl-th\]](https://arxiv.org/abs/0911.3346).
- [68] S. Goriely, N. Chamel, and J. M. Pearson. “Further Explorations of Skyrme-Hartree-Fock-Bogoliubov Mass Formulas. XII: Stiffness and Stability of Neutron-Star Matter”. In: *Physical Review C* 82 (2010), p. 035804. DOI: [10.1103/PhysRevC.82.035804](https://doi.org/10.1103/PhysRevC.82.035804). arXiv: [1009.3840 \[nucl-th\]](https://arxiv.org/abs/1009.3840).
- [69] J. M. Pearson, S. Goriely, and N. Chamel. “Properties of the Outer Crust of Neutron Stars from Hartree-Fock-Bogoliubov Mass Models”. In: *Physical Review C: Nuclear Physics* 83.6 (June 2011), p. 065810. DOI: [10.1103/PhysRevC.83.065810](https://doi.org/10.1103/PhysRevC.83.065810).
- [70] J. M. Pearson et al. “Inner Crust of Neutron Stars with Mass-Fitted Skyrme Functionals”. In: *Physical Review C* 85 (2012), p. 065803. DOI: [10.1103/PhysRevC.85.065803](https://doi.org/10.1103/PhysRevC.85.065803). arXiv: [1206.0205 \[nucl-th\]](https://arxiv.org/abs/1206.0205).
- [71] A. Y. Potekhin et al. “Analytical Representations of Unified Equations of State for Neutron-Star Matter”. In: *Astronomy and Astrophysics* 560 (2013), A48. DOI: [10.1051/0004-6361/201321697](https://doi.org/10.1051/0004-6361/201321697). arXiv: [1310.0049 \[astro-ph.SR\]](https://arxiv.org/abs/1310.0049).

- 
- [72] J. M. Pearson et al. “Unified Equations of State for Cold Non-Accreting Neutron Stars with Brussels–Montreal Functionals – I. Role of Symmetry Energy”. In: *Mon. Not. Roy. Astron. Soc.* 481.3 (2018), pp. 2994–3026. DOI: [10.1093/mnras/sty2413](https://doi.org/10.1093/mnras/sty2413), [10.1093/mnras/stz800](https://doi.org/10.1093/mnras/stz800). arXiv: [1903.04981](https://arxiv.org/abs/1903.04981) [astro-ph.HE].
  - [73] Michael Bender, Paul-Henri Heenen, and Paul-Gerhard Reinhard. “Self-Consistent Mean-Field Models for Nuclear Structure”. In: *Reviews of Modern Physics* 75.1 (2003), pp. 121–180. DOI: [10.1103/RevModPhys.75.121](https://doi.org/10.1103/RevModPhys.75.121).
  - [74] J. R. Stone and P. -G. Reinhard. “The Skyrme Interaction in Finite Nuclei and Nuclear Matter”. In: *Progress in Particle and Nuclear Physics* 58.2 (2007), pp. 587–657. DOI: [10.1016/j.ppnp.2006.07.001](https://doi.org/10.1016/j.ppnp.2006.07.001). arXiv: [nucl-th/0607002](https://arxiv.org/abs/nucl-th/0607002).